JOURNAL OF AIRCRAFT
Vol. 43, No. 3, May–June 2006

Transonic Free-to-Roll Analysis of the F-35 (Joint Strike Fighter) Aircraft

D. Bruce Owens*
NASA Langley Research Center, Hampton, Virginia 23681
Jeffrey K. McConnell†
Lockheed Martin Aeronautics Company, Fort Worth, Texas 76101
and
Jay M. Brandon‡ and Robert M. Hall‡
NASA Langley Research Center, Hampton, Virginia 23681

The free-to-roll technique is used as a tool for predicting areas of uncommanded lateral motions. Recently, the NASA/Navy/Air Force Abrupt Wing Stall Program extended the use of this technique to the transonic speed regime. Using this technique, this paper evaluates various wing configurations on the Joint Strike Fighter (F-35) aircraft. The configurations investigated include leading- and trailing-edge flap deflections, leading-edge flap gap seals, and vortex generators. These tests were conducted in the NASA Langley 16-Foot Transonic Tunnel. The analysis used a modification of a figure of merit developed during the Abrupt Wing Stall Program to discern configuration effects. The results showed how the figure of merit can be used to schedule wing flap deflections to avoid areas of uncommanded lateral motion. The analysis also used both static and dynamic wind-tunnel data to provide insight into the uncommanded lateral behavior. The dynamic data were extracted from the time history data using parameter identification techniques. In general, sealing the gap between the inboard and outboard leading-edge flaps on the Navy version of the F-35 eliminated uncommanded lateral activity or delayed the activity to a higher angle of attack.

Nomenclature

b_{ref}	=	reference wing span
C_L	=	lift coefficient
C_l	=	rolling-moment coefficient
$C_{l\text{rms}}$	=	rolling-moment coefficient rms
c_{ref}	=	reference wing chord (mean geometric chord)
M	=	Mach number
$p_{P\text{-}V}$	=	free-to-roll figure of merit
Re	=	Reynolds number based on c_{ref}
S	=	reference surface area
t	=	time
V_∞	=	freestream velocity
α	=	angle of attack
β	=	angle of sideslip
δ_e	=	symmetric horizontal tail deflection
δ_{ILEF}	=	inboard leading-edge flap deflection
δ_{LEF}	=	leading-edge flap deflection
δ_{OLEF}	=	outboard leading-edge flap deflection
δ_{TEF}	=	trailing-edge flap deflection
θ	=	pitch angle
ϕ	=	roll angle
ϕ_0	=	initial roll angle
$\dot{\phi}$	=	roll rate, time derivative of the roll angle
$\ddot{\phi}$	=	roll acceleration, time derivative of the roll rate

Presented as Paper 2004-5053 at the AIAA Atmospheric Flight Mechanics Conference and Exhibit, Providence, RI, 16–19 August 2004; received 5 April 2005; revision received 20 June 2005; accepted for publication 27 June 2005. This material is declared a work of the U.S. Government and is not subject to copyright protection in the United States. Copies of this paper may be made for personal or internal use, on condition that the copier pay the $10.00 per-copy fee to the Copyright Clearance Center, Inc., 222 Rosewood Drive, Danvers, MA 01923; include the code 0021-8669/06 $10.00 in correspondence with the CCC.

*Aerospace Engineer. Associate Fellow AIAA.
†Aeronautical Senior Staff Engineer. Member AIAA.
‡Senior Research Engineer. Associate Fellow AIAA.

I. Introduction

UNCOMMANDED lateral motions (wing drop/rock) plague many aircraft both in the low-speed high angle of attack (AoA) and high-speed moderate AoA flight regimes.[1] The free-to-roll (FTR) technique has been used for many decades to address the low-speed problems at a number of test facilities. Application of FTR in the transonic regime has been much more limited, but some testing was performed in Russia at the Sibnia Aerodynamic Research and Development Division[2] and in a semi-free-to-roll test conducted by Northrop and NASA Ames for the F-5A (see Ref. 3). More recently, the NASA/Navy/Air Force Abrupt Wing Stall (AWS) Program used the technique to assess uncommanded lateral activity on four military aircraft. The results of these free-to-roll tests as well as static force and moment, computational fluid dynamics (CFD), simulation, and flight tests are reported in Refs. 4–21. The current analysis will focus on the use of wind-tunnel data to identify configurations that improve lateral transonic flying qualities. The ideal case would be to use the wind-tunnel data results, along with data derived from CFD and other analytical sources, to model the unsteady aerodynamics for a piloted simulation study. This type of analysis, as recommended by Cook et al.,[20] would give a more comprehensive assessment of the flying qualities but is beyond the scope of this paper.

Early in the system demonstration and development phase of the F-35 Joint Strike Fighter (JSF) Navy variant, several warning signs were seen in the static wind-tunnel data, indicating the potential for wing drop at transonic Mach numbers. These signs included abrupt shifts in rolling moment, lift inflections, rolling-moment offsets, and poor data repeatability. Based on these observations, Lockheed Martin began coordinating closely with the ongoing AWS effort to take full advantage of the knowledge and expertise that had been developed as part of that program. Because the F-35 program was in the midst of an extensive wind-tunnel test program at that time, one particularly relevant aspect of the AWS program was the research done to develop a reliable technique for predicting wing drop from static wind-tunnel testing. The need for such a technique was highlighted during the preproduction F/A-18E/F program, where the lack of a reliable wind-tunnel-based method for predicting wing

drop forced the evaluation of potential fixes to be done almost entirely through flight test. Although several static wind-tunnel-based figures of merit were evaluated under the AWS program, this effort met with only limited success. By contrast, the transonic FTR technique, also developed under the AWS program, provided outstanding correlation to flight-test results for a range of configurations. Ultimately, the AWS program recommended FTR as the primary means of verifying that a new aircraft design is wing drop free.

Unfortunately, static wind-tunnel testing was the only practical method for performing rapid aerodynamic evaluation available to the JSF program given the number of configurations and the range of flight conditions to be considered. With this in mind, Lockheed Martin elected to channel resources into developing a technique for identifying potential wing-drop problems based solely on conventional force and moment testing. The end result of this effort is the continuous beta sweep test and analysis technique (CBSTAT), which is described in detail in Ref. 22. Using CBSTAT as the primary evaluation criteria, several potential design options were investigated to help understand and correct the aerodynamic deficiencies seen in the transonic Mach, moderate AoA flight regime. The source of the problem was eventually traced to a gap between the inboard and outboard leading-edge flap (LEF) at the wing fold. An aircraft level trade study was then launched to identify and implement potential fixes. This study led to a modification of the carrier-version (CV) LEF arrangement that allowed the gap to be sealed in flight while maintaining the required wing-fold capability. Subsequent CBSTAT-based evaluations of the modified configuration indicated that the sealed gap successfully resolved the wing-drop concerns. However, because previous efforts to establish a correlation between static-test-based wing-drop predictions and flight-test results had been unsuccessful, additional verification of the proposed solution was warranted. A FTR test was therefore added to the JSF test program to validate CBSTAT and to affirm that the configuration changes made to the CV variant did improve the lateral characteristics. To further explore the validity of CBSTAT, it was also applied to the preproduction F/A-18E and Harrier II configurations in separate wind-tunnel tests. The analyses of these wind-tunnel tests are presented in Refs. 23 and 24. Reference 25 presents the correlation of CBSTAT and FTR to flight-test results.

This paper analyzes the effect of configuration changes on the lateral activity of a 1/15th-scale F-35 aircraft model using the FTR technique at transonic speeds. For the JSF model, data for both the conventional takeoff and landing (CTOL) and CV variants will be analyzed with special emphasis on how the modified CV wing compares to the baseline configuration. The paper will show only aerodynamic effects because control system effects were not modeled. The time histories of the uncommanded lateral activity will be analyzed using static force and moment data as measured by the internally mounted six-component strain-gauge balance and dynamic data extracted from the roll-angle time histories using parameter identification (PID) methods.

II. FTR Test Technique

The FTR test technique is a single-degree-of-freedom method where the model is constrained to roll about the longitudinal body axis. When testing in this mode the rotary section of the FTR rig, the sting, the balance, and the model all rotate on two sets of low friction bearings in response to the aerodynamic rolling moments exerted on the model. The rolling motion can be described by a combination of forcing functions, roll damping C_{l_p}, and lateral stability C_{l_β} effects. Therefore, it is instructive when analyzing the data from a FTR test to consider the equation of motion in terms of the Euler angle ϕ as

$$I_x\ddot{\phi}/qSb + C_{l_{\dot{\phi}}}(\dot{\phi}b/2V_\infty) + C_{l_\phi}\phi = C_{l_0}$$

The foregoing equation is in the form of the classical mass-spring-damper system, where C_{l_0} represents an aerodynamic forcing function; C_{l_ϕ} represents the spring constant which, along with the inertia, determines the frequency of oscillation; and $C_{l_{\dot{\phi}}}$ represents the damping coefficient. In the FTR technique, the use of $C_{l_{\dot{\phi}}}$ and C_{l_p} is kinematically equivalent. By measuring roll angle vs time, the FTR technique captures the composite effect of both static and dynamic forces acting on the model regardless of whether they are steady or unsteady.

The top-level analysis from FTR testing involves assessing the severity of lateral activity (rolling motion). Because the models are typically not dynamically scaled, it is difficult to draw the line between acceptable and unacceptable lateral activity based solely on the behavior of the model. Therefore the severity of the lateral activity is assessed using the flight-data-correlated FTR figure of merit (FOM) that was developed during the AWS program.[14] The FTR FOM is computed from a time history of the roll angle using the following procedure. First, the absolute value of the amplitude change from a local maximum (peak) to its nearest local minimum (valley) is determined. Then, this value is divided by the time it takes to roll through this amplitude change. This ratio is, of course, the slope of a line connecting the maximum to the subsequent minimum. This quotient is computed for all of the maximums and minimums in a time history, and the final FTR FOM $p_{p\text{-}v}$ is selected as the highest of these ratios. In Ref. 14, this ratio was retained as a dimensional number, but for this paper the ratio is nondimensionalized using $b/2V_\infty$ to make the acceptable thresholds more generally applicable. Mathematically stated as

$$p_{P\text{-}V} \equiv [|\Delta\phi/\Delta t|(b/2V_\infty)]_{\max}$$

The threshold for this figure of merit was established as $p_{p\text{-}v} > 0.002$ through correlation to flight data that showed significant lateral activity. This FOM is not intended to indicate the type of motion, how long it took for the motion to develop, or how often the events happened. However, it has proven to be an accurate indicator of where uncommanded lateral motion will occur in flight and serves as conservative first filter for assessing the severity of the motion.

In practice, the FTR technique is an extension of static force and moment testing. The technique is used to evaluate the unsteady aerodynamic effects that time-averaged static force and moment data do not accurately capture. Also, the FTR technique captures roll damping effects that cannot be obtained in static testing. The primary data from the FTR technique are the roll-angle time history from which roll rate and roll acceleration can be determined. Knowing the roll acceleration and the inertia of the system, the total aerodynamic rolling moment can be computed. Of the static data, $C_l(\beta)$ or $C_l(\phi)$ are the most useful for understanding the FTR motions. These data indicate rolling-moment forcing functions and lateral stability (spring) effects. When available, $C_{l_{\text{rms}}}$ data can provide insight into the level of unsteadiness but do not quantify rolling-moment rate of change. The lift curve indicates areas where the wing flow topology is changing. It gives the α at which the wings are stalling but does not tell if the stall is asymmetric. If a rolling-moment offset is at the same α as wing stall, then the probability of a lateral motion is increased. If the lateral activity occurs during significant reduction in lift (i.e., a negative lift-curve slope), then a loss in roll damping can be expected. Therefore, the FTR and static tests are collaborated to provide a better understanding of the uncommanded lateral activity.

Because friction and inertia tend to subdue the lateral motion during FTR testing, efforts are made to minimize these effects. Large roll inertia makes the model less sensitive to changes in lateral aerodynamic asymmetries, making it difficult to resolve differences in configurations with small values of $p_{p\text{-}v}$. Friction adds artificial damping to the system. The FTR rig is designed to minimize friction, but this force is difficult to predict or model because it tends to be a function of the force acting normal to the roll axis bearings. Efforts have been made to quantify the friction effects, but thus far the accuracy of these calculations has not been entirely satisfactory. A separate research effort has been initiated to address the friction issues.

III. Wind-Tunnel Tests

A. Model

A 1/15th-scale model of the JSF (Fig. 1) was tested in the NASA Langley 16-Foot Transonic Tunnel (16-ft TT). The model was not

Fig. 1 Sketch of the 1/15th-scale baseline CV model of the JSF. $S_{ref} = 2.76$ ft^2, $b_{ref} = 2.87$ ft, and $c_{ref} = 1.113$ ft.

dynamically scaled. The issues of dynamic scaling are addressed in Refs. 14, 26, and 27. The CTOL and CV versions of the JSF model were tested. No variations to the CTOL model were tested. Numerous modifications to the CV model were assessed. On the CV model, the baseline wing had an inboard and outboard LEF that had different hinge lines (Fig. 1). When the LEF was deflected, the outboard section would be at a higher deflection than the inboard and will be denoted in the discussion as $\delta_{LEFI}/\delta_{LEFO}$ in degrees. The LEF deflections tested on the baseline wing were 10/12.4, 12.5/15.5, 16/19.8, and 20/24.8. There was also a gap between the inboard and outboard LEF sections on the baseline CV such that the two were not touching and moved independently. Prior to the FTR test, CBSTAT evaluation showed that sealing this gap eliminated deficiencies in the static lateral characteristics, which were considered to be indicators of wing drop. To facilitate the closing of this gap, a modification to the configuration was developed, which involved using a common hinge line for both the inboard and outboard flap and maintaining equivalent deflections. To model this in the wind tunnel, separate parts were used for the inboard and outboard LEFs, but the gap was sealed with dental plaster and tape. This nonpermanent seal was selected to permit investigations to be conducted with the gap open, partially open, and fully sealed. The wing with the common hinge line and sealed gap, which will simply be referred to as the "new wing," was tested at LEF deflections of 10, 12, and 16 deg.

Many other parameters were varied during the JSF testing to understand the influence of various configuration changes. These parameters included trailing-edge-flap (TEF) deflection, symmetric aileron deflection, horizontal-tail deflection, vortex-generator (VG) arrays on the outer wing panels, removing the transition trip dots, and beveling the inboard face of the outboard LEF. The model was tested over the speed range $0.60 \leq M \leq 0.98$ with a corresponding Reynolds number variation of 3.7 to 4.1 $\times 10^6$ based on c_{ref}.

The 16-ft TT wind-tunnel tests consisted of a static force and moment phase and a FTR phase. For both phases the model was tested on the FTR rig as shown in Fig. 2. During the static force and moment testing, a locking bar was placed across the stationary and rotary sections of the FTR rig, and data were measured using an internally mounted six-component strain-gauge balance. The static data were taken in a point-pause mode. In this mode the model was held at a fixed condition, and 50 samples were acquired over a 5-s window then averaged to create a single data point. This paper also presents data from a JSF static force and moment test conducted in

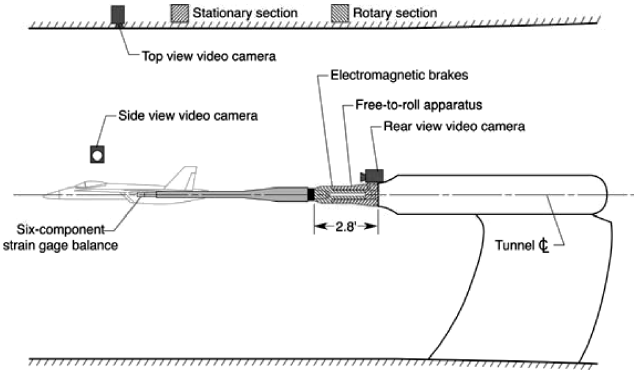

Fig. 2 Sketch of the NASA Langley 16-ft TT FTR apparatus.

the Veridian Transonic Wind Tunnel. These data were also measured using an internally mounted six-component strain-gauge balance but were acquired during continuous β sweeps performed at a sweep rate of 0.33 deg/s. During the 16-ft TT FTR tests, the roll-angle time history was measured using a resolver with an accuracy of 0.067 deg. The roll-angle signal was captured at a rate of 200 Hz using a 4-Hz analog filter. The strain-gauge balance signals were recorded at 50 Hz using a 10-Hz analog filter, and video of the rolling motions was recorded.

During the FTR test phase, three test methods are employed to investigate the potential for lateral activity: continuous pitch sweep, pitch pause with $\phi_0 = 0$ deg, and pitch-pause with $\phi_0 \neq 0$ deg. Reference 14 provides a detailed description of the procedures for conducting FTR testing using each of these methods. Unlike static force and moment testing where α and β are standard model attitude variables, FTR testing uses θ and ϕ as the primary independent variables. When the parameter α is used to compare static and FTR data, without stating a specific β, then it is implied that $\beta = 0$ deg in both types of data.

B. Roll Damping Derivative Estimation Method

The roll damping derivative C_{lp} given in this paper was estimated using PID methods. The method used in the current analysis is based on linear regression performed using a package of MATLAB® scripts developed at NASA Langley called SIDPAC.[28] The FTR motions were modeled in this approach using the governing equation just given assuming constant coefficients over a specified range of ϕ. Also, note that the actual parameter that was computed is $C_{l_p} + C_{l_\beta} \sin\alpha$ caused by the body-axis motion.

IV. Results and Discussion

The CTOL and CV configurations of the JSF were tested over a large M-α-β-δ_{LEF} space. The FTR FOM will be the starting point for the discussion with the use of static and dynamic data to explain the effect of modifying the baseline configuration. For the CV variant, the data will show the effect of sealing the LEF gap at the wing-fold junction, partially sealing this gap, vortex generators, beveling the inboard face of the outboard LEF, the effect of deflecting the horizontal tail, and the use of $p_{p\text{-}v}$ for flap scheduling.

A. CTOL Configuration

The CTOL configuration was evaluated using the FTR technique for $0.6 \leq M \leq 0.95$ and $\delta_{LEF} = 13$, 16, and 20 deg. In general, this configuration demonstrated benign lateral activity. An example of the level of lateral activity of the CTOL model with $\delta_{LEF} = 16$ deg is shown in Fig. 3. The plot shows little to no activity over the tested Mach range. What activity that did exist was considered to be inconsequential as it was well off of the baseline flap schedule. The plot also presents a repeat point at $M = 0.9$ as an indication of the resolution of $p_{p\text{-}v}$. Figure 4 presents the FTR FOM for the three LEF deflections tested at $M = 0.8$ and shows that it would be relatively easy to schedule the LEF to avoid the limited regions of uncommanded lateral activity. CBSTAT evaluations conducted

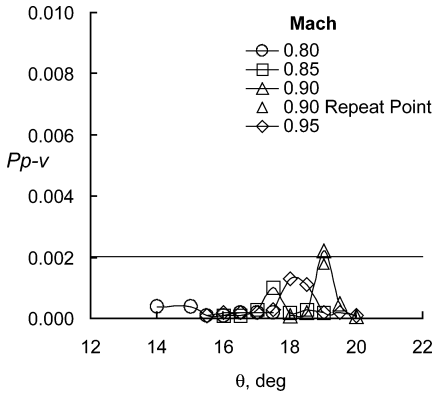

Fig. 3 Effect of Mach number on the lateral activity of the CTOL configuration for $\delta_{LEF} = 16$ deg.

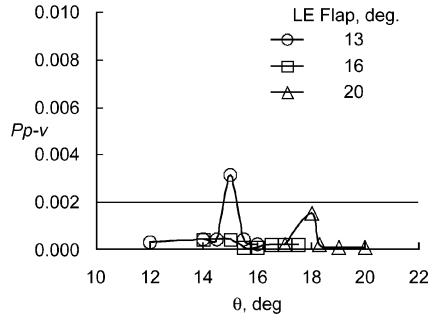

Fig. 4 Effect of flap deflection on the lateral activity of the CTOL configuration for $M = 0.8$.

prior to the FTR test showed that the lateral aerodynamics of the CTOL were well behaved. Based on these benign CBSTAT results, no modification was thought to be required for this variant, and so no alternate configurations were built for the model. The low-level of lateral activity on the FTR rig correlated well with these results and affirmed that wing drop was not likely to be a problem for the CTOL variant.

B. CV Configuration

1. Effect of Mach Number

The CV model was tested over the Mach range $0.60 \leq M \leq 0.98$. At $M = 0.60$, the model did not exhibit any significant lateral activity for the configurations tested. At $0.70 \leq M \leq 0.92$, significant lateral activity was observed in the form of wing rock/drop. For $0.92 < M \leq 0.96$, the model tended to trim at a large roll angle as a result of the lateral stability at these conditions. At some pitch attitudes, the model would trim at one ϕ for a period of time then abruptly change to trim at a significantly different ϕ. This unusual behavior was attributed to the fact that the stability of the configuration was neutral or slightly unstable at small sideslips but became stable as β increased. As the model rolled at a fixed θ, β increased until a trim point in C_l was achieved. Because of the weak lateral stability, even relatively small unsteady jumps in rolling moment would cause the model to transition to an entirely different trim point. For the limited cases that were obtained at $0.96 < M \leq 0.98$, the model did not exhibit significant lateral activity, and the static lateral stability was stable and more linear than at $0.92 < M \leq 0.96$. For all of the Mach numbers tested, FTR results were consistent with the CBSTAT predictions developed from static test data taken in other tunnels prior to the test. The effect of Mach number just described holds true regardless of the modifications tested on the CV model.

2. Effect of Sealing the LEF Gap

During static force and moment testing on the JSF CV model, aerodynamic anomalies such as hysteresis, unsteadiness, and poor repeatability were observed at several flight conditions. The regions exhibiting these unfavorable characteristics were initially identified using continuous β-sweep testing conducted as part of the CBSTAT wing-drop evaluation technique. Once found, a variety of test methods including oil flow visualization, dwell testing, and wing-root bending moment analysis were used to further understand and isolate the source of these anomalies. Oil flow visualization of the upper wing surface was conducted for a range of sideslips. This showed that the problems were caused primarily by a gap between the inboard and outboard LEFs that occurred at the wing-fold location.

At some conditions it appeared that a vortex emanating from the LEF gap acted like a wing fence that prevented spanwise flow from the inboard section of the wing from degrading flow outboard of the wing fold. At specific combinations of Mach, α, and β, the vortex would burst, and the outer wing panel would stall abruptly resulting in a sudden change in rolling moment. At other conditions similar jumps in rolling moment were observed as a shock, which normally affixed itself near the TEF hinge line, would migrate forward on the wing rapidly and attach itself to the LEF gap. When the shock jumped to the more forward position, a significant reduction in lift would occur on the wing as the flow behind the shock was separated. Again, this sudden lift loss would produce rapid rolling-moment changes that would undoubtedly lead to wing drop in flight.

On the FTR rig either of the two events just described above would act as triggering mechanisms for the onset of lateral activity. The unsteady nature of these flow changes was seen in the variety of roll motions observed during FTR testing. In some cases multiple large-amplitude wing drops were observed as the model would roll suddenly to a large amplitude, return to zero bank, then experience another drop in the same, or opposite, direction. On other runs the model would sit still for extended periods of time before being upset by a sudden asymmetric rolling moment. At the most severe conditions the model would diverge immediately after brake release and exhibit large-amplitude wing rock for the remainder of the time history.

Figure 5 shows the location and picture of the LEF gap. In general for $0.7 \leq M \leq 0.9$ and $10 \text{ deg} \leq \delta_{LEF} \leq 20$ deg, the effect of sealing the gap was to reduce the severity and delay or eliminate the onset of significant lateral activity over the α range tested. An example is shown in the FTR FOM plot of Fig. 6. The figure shows that the baseline wing had significant activity over the range $8 \text{ deg} \leq \alpha \leq 16$ deg (with the exception of $\alpha = 13$ and 13.5 deg), which is classified as severe wing rock. At $\alpha = 8$, 10, 14, and 15 deg, the lateral activity occurred even from releasing the model at a $\phi_0 = 0$ deg initial condition. For $\alpha = 11$, 12, and 16 deg, the model did not show any significant lateral motion when released from a wings-level condition but did exhibit sustained, violent wing rock when the motion was initiated by releasing the model at a nonzero bank angle.

In general, the effect of sealing the gap and having a constant LEF deflection for the entire wing span reduced or eliminated unsteady rolling moments, decreased static lateral stability, increased roll damping, and caused an earlier break in the lift curve. The static lateral stability, roll damping, and the type of lateral activity were

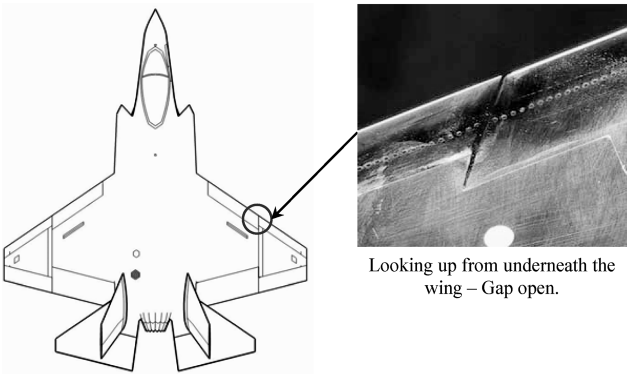

Fig. 5 Sketch of JSF CV model showing the gap between the inboard and outboard LEF. Also shown are the trip dots.

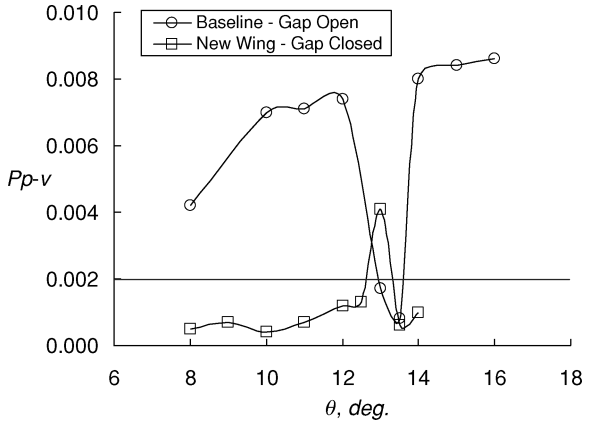

Fig. 6 Effect of sealing the gap on the lateral activity of the JSF CV model at $M = 0.85$ (Baseline, $\delta_{LEF} = 12.5$ deg/15.5 deg; new wing; $\delta_{LEF} = 12.5$ deg).

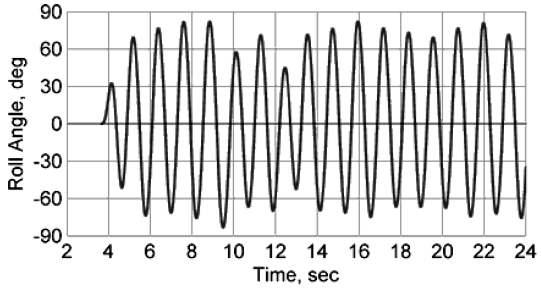

Fig. 7a Roll-angle time history of the baseline with $\delta_{LEF} = 12.5$ deg/15.5 deg at $\theta = 10$ deg and $M = 0.85$.

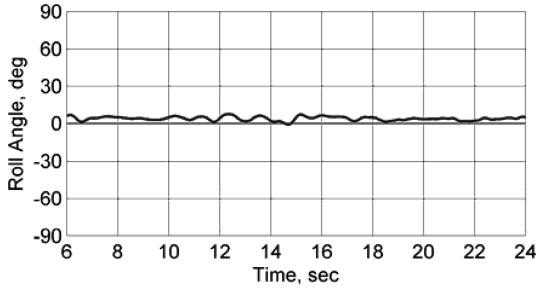

Fig. 7b Roll-angle time history of the new wing with $\delta_{LEF} = 12.5$ deg at $\theta = 10$ deg and $M = 0.85$.

similar for 9 deg $\leq \alpha \leq$ 12 deg. An example time history for these conditions is shown in Fig. 7 at $\theta = 10$ deg. The pronounced effect of sealing the LEF gap is easily seen by contrasting the severe wing rock of the baseline configuration with the benign activity of the new wing.

Insight into the aerodynamic causes of the baseline configuration lateral activity can be obtained from the static and dynamic data shown in Figs. 8 and 9. The C_l vs β plot shown in Fig. 8 was collected during a series of continuous β sweeps performed at constant α by sweeping from $\beta = -10$ to 10 deg then back again over the same range in the opposite direction. The plot shows that a large hysteresis loop exists for the baseline configuration between -4 and $+3$ deg, which is β not present when the gap is sealed. These hysteresis loops indicate that there are multiple stable flow states at these conditions. This was confirmed by performing dwell testing inside these hysteresis loops, which showed that multiple values of C_l can occur with no measurable variation in test condition. During FTR testing at $\alpha = 10$ deg and $\phi_0 = 0$ deg, the model immediately developed limit-cycle wing rock (Fig. 7a) even though the model was statically stable for -10 deg $\leq \beta \leq 10$ deg (which is the range of β experienced during the wing rock). This behavior is explained by the combined effect of the unsteady, multivalued rolling moments at low β and the unstable C_{lp} at $\alpha = 10$ deg shown in Fig. 9. After being released at $\phi_0 = 0$ deg, the model evidently experienced an asymmetric flow topology change, which triggered the rolling motion. Once started, a limit-cycle wing rock ensues because of the unstable roll damping near $\beta = 0$ deg, stable $C_{l\beta}$, and a forcing function shown by the hysteresis loop shown in Fig. 8.

Further examination of Figs. 8 and 9 can also explain why the baseline configuration showed much lower levels of lateral activity around $\alpha = 13$ deg than in the 8- to 12-deg region in Fig. 6. Unlike the other α shown, the $\alpha = 13$-deg data in Fig. 8 do not exhibit any hysteresis for the open gap configuration near $\beta = 0$ deg. In addition, Fig. 9 shows that the baseline configuration has marginal dynamic stability around $\alpha = 13$ deg. Therefore, the static and dynamic data support the absence of significant activity at $\alpha = 13$ deg seen on the FTR rig when the model is released with no roll rate at an initial condition of $\beta = \phi = 0$ deg. However, because hysteresis loops do exist beyond $\beta = \pm 2.5$ deg and C_{lp} is nearly neutral, the possibility for lateral activity does exist and can well occur if the baseline configuration were given a roll rate by releasing it at a nonzero ϕ. Unfortunately, a bank and release run was not performed at this test condition.

As shown in the FTR FOM plot of Fig. 6, the new wing had no significant lateral activity except at $\alpha = 13$ deg. Relative to the baseline, the new wing also eliminated the hysteresis loops in static rolling moment (Fig. 8) and increases roll damping (Fig. 9) significantly except at $\alpha = 13$ deg. Based on these changes, it appears that the FTR activity at $\alpha = 13$ deg can be attributed to the nonlinearities in rolling moment near $\beta = 0$ deg (Fig. 8) and the localized reduction in roll damping at this condition.

To further understand the effect of the gap, sensitivity to the chordwise length of the gap was briefly evaluated using continuous pitch-up sweeps. For this investigation the width of the gap was not varied, but it was filled in starting from the downstream end such that approximately two-thirds of the gap was closed. The FTR FOM results in Fig. 10 for $0.70 \leq M \leq 0.90$ show that the level of lateral activity is highly sensitive to the gap depth. This finding indicates that a robust design that completely seals the gap is required to avoid wing drop. Note that the summary shown in Fig. 10 presents the maximum value of p_{p-v} for the entire pitch sweep range rather than the pitch-pause points that are normally used when calculating p_{p-v}. Continuous pitch-up sweeps were used frequently during the test as a means of quickly screening a new configuration. The FTR FOM plot does not show at which θ the peak p_{p-v} value occurred at, but this θ was approximately the same for both configurations at each Mach that was evaluated. The reason for using the FOM plot rather than showing roll-angle time-history plots is that it succinctly captures the effect of partially sealing the gap for $0.7 \leq M \leq 0.90$. It would require the use of 12 time-history plots to show the breadth of information contained in this one plot.

3. *Effect of LEF Gap Geometry*

The inward face of the outboard LEF was flat for the results just shown. On the full-scale aircraft this face would be beveled. Therefore, a short investigation of this geometry change was conducted. Figure 11 shows the effect of the beveled flap edge on the lateral activity for $0.6 \leq M \leq 0.9$ with $\delta_{LEF} = 12.5$ deg using the FTR FOM. The $p_{p\text{-}v}$ is computed from continuous pitch-up sweeps using the maximum value of $p_{p\text{-}v}$ over the entire pitch range. As the plot shows, there is no effect of the beveled edge except at $M = 0.9$, where the value of $p_{p\text{-}v}$ is twice that for the flat face.

4. *Effect of VGs*

One alternative to sealing the gap, which showed some promise in static wind-tunnel testing, involved placing three VGs on the outer wing panel. Figure 12 presents the effect of VGs on the lateral activity along with a picture showing the location of the VGs as viewed looking outboard along the left wing. The $p_{p\text{-}v}$ is computed from continuous pitch-up sweeps using the maximum value of the $p_{p\text{-}v}$ over the entire pitch range. Results indicate that the VGs actually caused significant increases in the lateral activity at $M = 0.60$ and

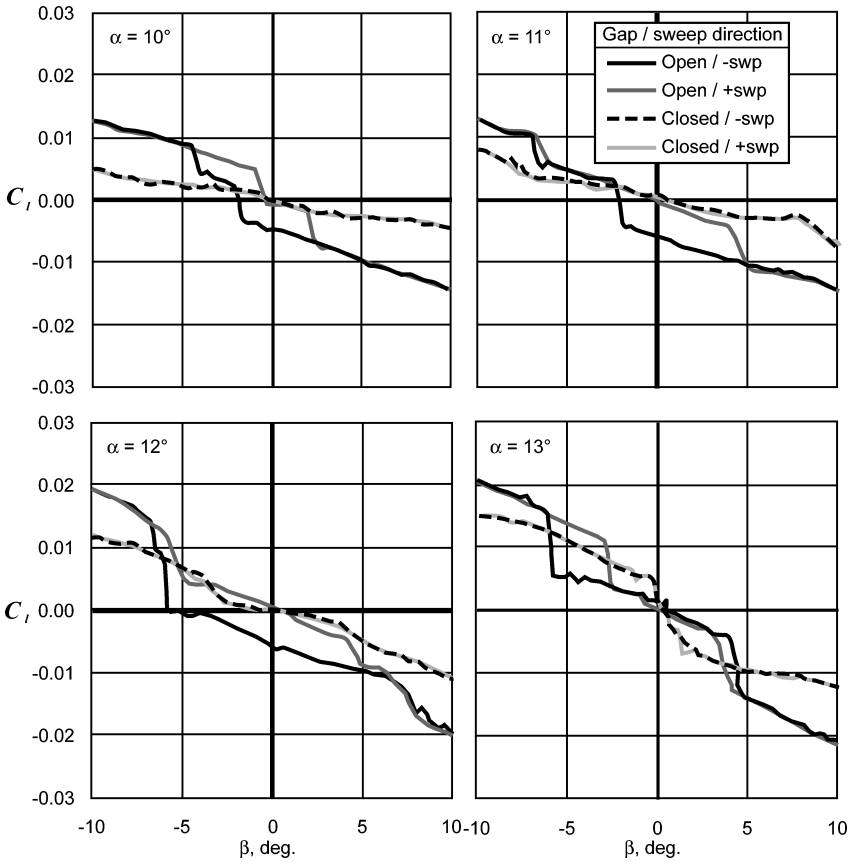

Fig. 8 Static rolling moment for the open gap case (baseline wing with $\delta_{LEF} = 12.5$ deg/15 deg) and closed gap case (new wing with $\delta_{LEF} = 12.5$ deg) at $M = 0.85$. In the legend −swp means the β sweep was from +10 to −10 deg, and +swp refers to −10 to +10 deg.

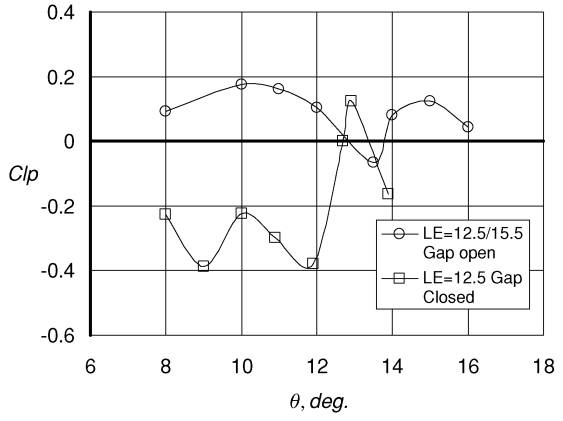

Fig. 9 Roll damping for the baseline ($\delta_{LEF} = 12.5$ deg/15.5 deg) and new wing ($\delta_{LE} = 12.5$ deg) at $M = 0.85$.

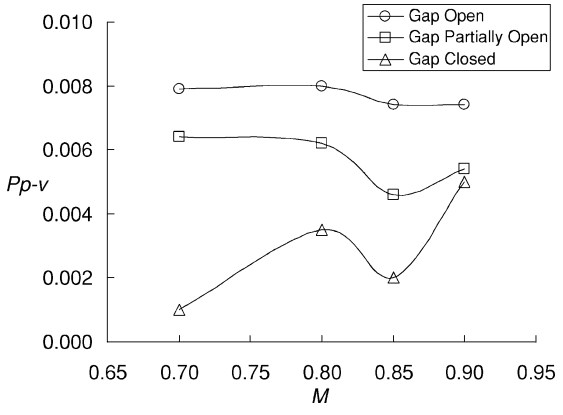

Fig. 10 Effect of partially sealing the gap. New wing with $\delta_{LEF} = 12.5$ deg.

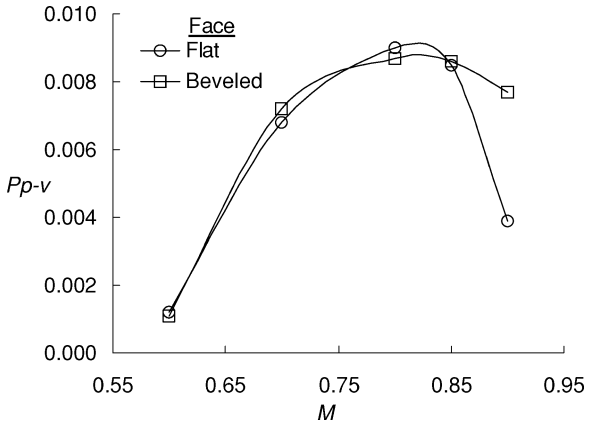

Fig. 11 Effect of beveling the inboard face of the outboard LEF on the lateral activity for the baseline wing with a $\delta_{LEF} = 12.5$ deg/15.5 deg.

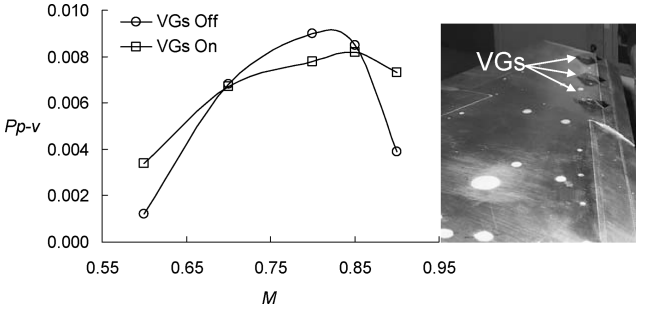

Fig. 12 Effect of VGs on the lateral activity for $0.60 \le M \le 0.90$ and $\delta_{LEF} = 12.5$ deg/15.5 deg. Inset—looking out the left wing showing the location of the three VGs.

0.90, have no effect at $M = 0.70$ and 0.85, and provide only a minor reduction in the level of lateral activity at $M = 0.80$. Based on these results, and the mixed data that were obtained during conventional force and moment testing, the VGs were considered to be a nonviable solution.

5. Effect of Horizontal Tail Deflection

Nearly all of the FTR testing was done with the horizontal tails set to 0-deg deflection, but a short test series was done to determine the effect of horizontal tail deflection on the level of lateral activity. Given the tail's close proximity to the wing (see sketch in Fig. 5), there was some concern that horizontal tail deflections can influence the wing aerodynamics thereby aggravating wing drop characteristics. Figure 13 shows the effect of symmetric horizontal tail deflections on the lateral activity for $0.7 \leq M \leq 0.90$ with the LEF gap sealed and $\delta_{\text{LEF}} = 10$ deg. The $p_{p\text{-}v}$ values, which again represent the maximum $p_{p\text{-}v}$ value observed during continuous pitch-up sweeps, show that deflecting the tail either decreased or had no considerable effect on the level of lateral activity. Therefore, assessing the wing-drop tendencies of the model with the horizontal tails undeflected is a conservative approach.

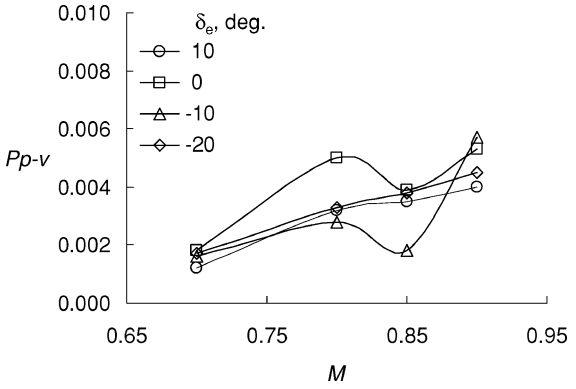

Fig. 13 Effect of horizontal tail deflection on the lateral activity of the new wing with $\delta_{\text{LEF}} = 10$ deg. LEF gap sealed.

6. Flap Scheduling

Because sealing the LEF gap did not completely eliminate the potential for wing drop/rock over the entire α range, some scheduling of the flaps will be required to avoid problem areas. Figure 14 shows the level of lateral activity, expressed as $p_{p\text{-}v}$, for three LEF deflections at $M = 0.70$, 0.80, 0.85, and 0.90. The plots clearly show that the peaks in lateral activity spread out in a predictable pattern with LEF deflection. That is, peak in lateral activity moves to a higher α as the deflection is increased. As with the CTOL variant, these results indicate that a reasonable schedule can be developed for the CV configuration to avoid flight conditions exhibiting significant levels of lateral activity.

V. Conclusions

This paper analyzes the effect of configuration changes on the FTR activity of a 1/15th-scale F-35 at transonic speeds. The CTOL and CV variant of the JSF were tested in the NASA Langley 16-Foot Transonic Tunnel. From the results, the CTOL variant should not exhibit uncommanded lateral activity on the nominal flap schedule. Even off-schedule conditions showed only moderate activity for a few M-α-δ_{LEF} combinations. For the CV variant, several configurations were tested at $0.6 \leq M \leq 0.98$ and subsequently analyzed. These configurations included sealing the LEF gap, LEF and TEF deflections, horizontal tail deflections, and vortex generators. In general, sealing the LEF gap reduced or eliminated unsteady rolling moments, decreased static lateral stability, increased roll damping, and caused an earlier break in the lift curve. The effect of the geometry inside the gap was also investigated and proved to have little effect on lateral activity except at $M = 0.90$. Vortex generators were investigated and found to be ineffective. Symmetric horizontal tail assessments showed that deflecting the tail decreased or had no considerable effect on the level of lateral activity. Finally, it was shown

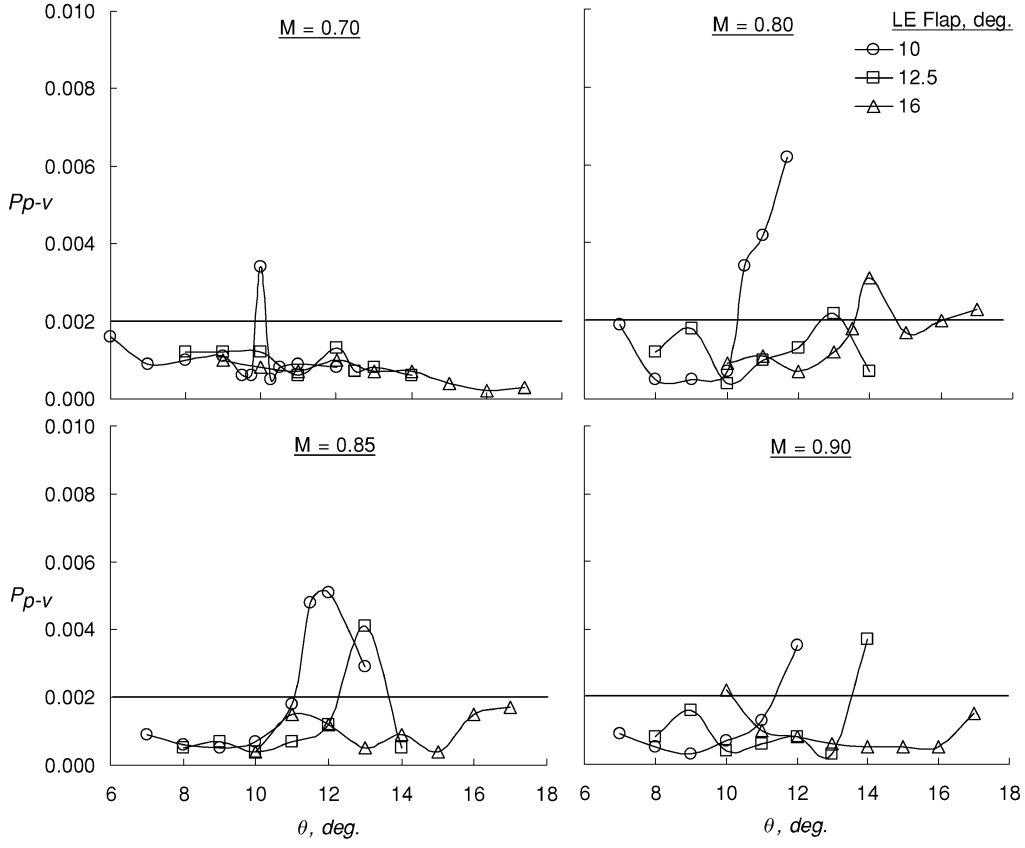

Fig. 14 Use of the FTR–FOM for determining flap schedule at $M = 0.70$, 0.80, 0.85, and 0.90.

using the FTR FOM that the peak in lateral activity moves to a higher α as the LEF deflection is increased. Therefore, LEF scheduling can be used to avoid any potential uncommanded lateral activity on the CV variant.

Acknowledgments

Naomi McMillian, Fran Capone, and Kevin Cunningham of NASA Langley Research Center and Steve Cook of Naval Air Systems Command, Patuxent River provided assistance with the wind-tunnel tests.

References

[1]Chambers, J., and Hall, R., "Historical Review of Uncommanded Lateral-Directional Motions at Transonic Conditions," *Journal of Aircraft*, Vol. 41, No. 3, 2004, pp. 436–447.

[2]Kashafutdinov, S., and Derishev, S., "Major Scientific Areas and Experimental Facilities of Sibnia Aerodynamic Research and Development Division," Siberian Aeronautical Research Inst., Novosibirsk, Russia.

[3]Hwang, C., and Pi, W., "Some Observations on the Mechanism of Aircraft Wing Rock," AIAA Paper 78-1456, Aug. 1978.

[4]Hall, R., and Woodson, S., "Introduction to the Abrupt Wing Stall (AWS) Program," *Journal of Aircraft*, Vol. 41, No. 3, 2004, pp. 425–435.

[5]McMillin, N., Hall, R., and Lamar, J., "Understanding Abrupt Wing Stall with Experimental Methods," AIAA Paper 2003-0591, Jan. 2003.

[6]Woodson, S., Green, B., Chung, J., Grove, D., Parikh, P., and Forsythe, J., "Understanding Abrupt Wing Stall (AWS) with CFD," AIAA Paper 2003-0592, Jan. 2003.

[7]Schuster, D., and Byrd, J., "Transonic Unsteady Aerodynamics of the F/A-18E at Conditions Promoting Abrupt Wing Stall," *Journal of Aircraft*, Vol. 41, No. 3, 2004, pp. 485–492.

[8]Forsythe, J., and Woodson, S., "Unsteady CFD Calculations of Abrupt Wing Stall Using Detached-Eddy Simulation," AIAA Paper 2003-0594, Jan. 2003.

[9]Parikh, P., and Chung, J., "A Computational Study of the AWS Characteristics for Various Fighter Jets: Part I, F/A-18E & F-16C," AIAA Paper 2003-0746, Jan. 2003.

[10]Chung, J., and Parikh, P., "A Computational Study of the Abrupt Wing Stall (AWS) Characteristics for Various Fighter Jets: Part II, AV-8B and F/A-18C," AIAA Paper 2003-0747, Jan. 2003.

[11]Lamar, J., Capone, F., and Hall, R., "AWS Figure of Merit (FOM) Developed Parameters from Static, Transonic Model Tests," AIAA Paper 2003-0745, Jan. 2003.

[12]Lamar, J., Hall, R., Capone, F., and McMillin, N., "Usefulness of Transonic Model Static Data in Predicting Flight Abrupt-Wing-Stall," *Journal of Aircraft*, Vol. 41, No. 3, 2004, pp. 464–473.

[13]Capone, F., Owens, B., and Hall, R., "Development of a Free-To-Roll Transonic Test Capability," *Journal of Aircraft*, Vol. 41, No. 3, 2004, pp. 456–463.

[14]Owens, B., Capone, F., Hall, R., Brandon, J., Cunningham, K., and Chambers, J., "Transonic Free-to-Roll Analysis of Abrupt Wing Stall on Military Aircraft," *Journal of Aircraft*, Vol. 41, No. 3, 2004, pp. 474–484.

[15]Roesch, M., and Randall, B., "Flight Test Assessment of Lateral Activity," AIAA Paper 2003-0748, Jan. 2003.

[16]Green, B., and Ott, J., "F/A-18C to E Wing Morphing Study for the Abrupt Wing Stall Program," AIAA Paper 2003-0925, Jan. 2003.

[17]Kokolios, A., Cook, S., and Niewoehner, R., "Use of Piloted Simulation for Evaluation of Abrupt Wing Stall Characteristics," AIAA Paper 2003-0924, Jan. 2003.

[18]Capone, F., Hall, R., Owens, B., Lamar, J., and McMillin, N., "Review and Recommended Experimental Procedures for Evaluation of Abrupt Wing Stall Characteristics," *Journal of Aircraft*, Vol. 41, No. 3, 2004, pp. 448–455.

[19]Woodson, S., Green, B., Chung, J., Grove, D., Parikh, P., and Forsythe, J., "Recommendations for CFD Procedures for Predicting Abrupt Wing Stall (AWS)," AIAA Paper 2003-0923, Jan. 2003.

[20]Cook, S., Chambers, J., Kokolios, A., Niewoehner, R., Owens, B., Page, A., and Roesch, M., "An Integrated Approach to Assessment of Abrupt Wing Stall for Advanced Aircraft," AIAA Paper 2003-0926, Jan. 2003.

[21]Hall, R., Woodson, S., and Chambers, J., "Accomplishments of the AWS Program and Future Requirements," AIAA Paper 2003-0927, Jan. 2003.

[22]McConnell, J., "Continuous Beta Sweep Test and Analysis Technique (CBSTAT) for Predicting Wing Drop Based on Static Wind Tunnel Testing," AIAA Paper 2004-5048, Aug. 2004.

[23]Kokolios, A., Gonzalez, H., Ghee, T., and Pettersson, H., "Analysis of Beta Hysteresis Figure of Merit on a Super Hornet Configuration," AIAA Paper 2004-5051, Aug. 2004.

[24]Payne, P., and McConnell, J., "Predicting Wing Drop on the Harrier II Using the Static Wind Tunnel Test and Analysis Technique CBSTAT," AIAA Paper 2004-5050, Aug. 2004.

[25]Cook, S., Gonzalez, H., Owens, B., McConnell, J., and Payne, P., "Correlation of the Continuous Beta Sweep Test and Analysis Technique to Transonic Free-to-Roll and Flight Test Results," AIAA Paper 2004-5052, Aug. 2004.

[26]Wolowicz, C. H., Bowman, J. S., and Gilbert, W. P., "Similitude Requirements and Scaling Relationships as Applied to Model Testing," NASA TP 1435, Aug. 1979.

[27]Brandon, J., and Foster, J., "Recent Dynamic Measurements and Considerations for Aerodynamic Modeling of Fighter Airplane Configurations," AIAA Paper 98-4447, Aug. 1998.

[28]Morelli, E., "System Identification Programs for Aircraft (*SIDPAC*)," AIAA Paper 2002-4704, Aug. 2002.